

Article

# Catalytic Activity of Beta-Cyclodextrin-Gold Nanoparticles Network in Hydrogen Evolution Reaction

Qui Quach, Erik Biehler, Ahmed Elzamzami, Clay Huff, Julia M. Long and Tarek M. Abdel-Fattah \* 

Applied Research Center, Thomas Jefferson National Accelerator Facility, Department of Molecular Biology and Chemistry, Christopher Newport University, Newport News, VA 23606, USA; qui.quach.13@cnu.edu (Q.Q.); erik.biehler.16@cnu.edu (E.B.); ahmed.elzamzami.17@cnu.edu (A.E.); clay.huff.12@cnu.edu (C.H.); julia.long.15@cnu.edu (J.M.L.)

\* Correspondence: fattah@cnu.edu

**Abstract:** The current climate crisis warrants investigation into alternative fuel sources. The hydrolysis reaction of an aqueous hydride precursor, and the subsequent production of hydrogen gas, prove to be a viable option. A network of beta-cyclodextrin capped gold nanoparticles (BCD-AuNP) was synthesized and subsequently characterized by Powder X-Ray Diffraction (P-XRD), Fourier Transform Infrared (FTIR), Transmission Electron Microscopy (TEM), and Ultraviolet-Visible Spectroscopy (UV-VIS) to confirm the presence of gold nanoparticles as well as their size of approximately 8 nm. The catalytic activity of the nanoparticles was tested in the hydrolysis reaction of sodium borohydride. The gold catalyst performed best at 303 K producing  $1.377 \text{ mL min}^{-1} \text{ mL}_{\text{cat}}^{-1}$  of hydrogen. The activation energy of the catalyst was calculated to be 54.7 kJ/mol. The catalyst resisted degradation in reusability trials, continuing to produce hydrogen gas in up to five trials.

**Keywords:** gold nanoparticles network; catalysts; hydrogen evolution; hydride precursors



**Citation:** Quach, Q.; Biehler, E.; Elzamzami, A.; Huff, C.; Long, J.M.; Abdel-Fattah, T.M. Catalytic Activity of Beta-Cyclodextrin-Gold Nanoparticles Network in Hydrogen Evolution Reaction. *Catalysts* **2021**, *11*, 118. <https://doi.org/10.3390/catal11010118>

Received: 9 December 2020

Accepted: 10 January 2021

Published: 15 January 2021

**Publisher's Note:** MDPI stays neutral with regard to jurisdictional claims in published maps and institutional affiliations.



**Copyright:** © 2021 by the authors. Licensee MDPI, Basel, Switzerland. This article is an open access article distributed under the terms and conditions of the Creative Commons Attribution (CC BY) license (<https://creativecommons.org/licenses/by/4.0/>).

## 1. Introduction

Since the industrial revolution, the advancement of technology has resulted in the need for a stable and eco-friendly energy source [1,2]. The Earth's fossil fuel supplies will be depleted in the near future, and have caused detrimental effects our environment, causing many scientists to seek clean and reliable fuel sources [3–5]. Hydrogen energy has been identified as a potential green alternative fuel source due to its abundance and environmentally friendly emission of water vapor upon combustion [6,7]. The production and application of hydrogen fuel technology has faced various challenges; from lacking clean sources to the dangers of current storage methods. Currently, the production of hydrogen fuel is expensive and requires the use of fossil fuels [8,9]. Additionally, hydrogen liquid needs to be stored under high pressure and at extremely low temperatures [7,10]. Hydrogen feedstock materials are an emerging class of chemicals that have the potential to replace the liquid and compressed gas methods of hydrogen storage. Sodium borohydride ( $\text{NaBH}_4$ ) has already been identified as a possible candidate due to its low weight and impressive hydrogen content of 10.8% wt. Additionally, this material readily releases hydrogen gas when it reacts with water [11]. However, this reaction proceeds very slowly and would require the addition of a catalyst to bring the hydrogen production to a rate efficient enough to be widely utilized [12–14].

Many previous metals and their composites have been applied in improving the hydrogen generation rate of  $\text{NaBH}_4$  due to their stability and high surface area [13–15]. Among those metals, gold nanoparticles (AuNPs) display interesting optical, electrical, and catalytic properties, and are considered one of the more active nanoparticle catalysts due to their lack of a stable oxide [16]. Additionally, previous studies have shown impressive catalytic activity of AuNPs in both reduction and also hydrogenation reactions [15,17,18]. However, the application of nanoparticles often faces problems with agglomeration that

can change the size and distribution of the nanoparticles [19]. Since precious metals are expensive, it is necessary to improve their stability and recyclability. In our work, beta-cyclodextrin was used as a capping agent during AuNP synthesis since previous research has shown that beta-cyclodextrin is capable of enhancing the shape, performance and stability of nanoparticles [13,14,20,21]. Additionally, the research of Osborn et.al., showed that the gold nanoparticles with a citrate capping agent had a significantly higher activation energy compared to gold nanoparticles supported over activated carbon [15]. In this research, we want to determine whether or not the use of beta-cyclodextrin as a capping agent can improve the activation energy of gold nanoparticles.

In our study, beta-cyclodextrin capped AuNPs networks (BCD-AuNPs) were synthesized and characterized by ultraviolet-visible spectroscopy (UV-VIS), powder x-ray diffraction (P-XRD), Fourier transform infrared (FT-IR), and transmission electron microscopy (TEM). The catalytic ability of obtained AuNPs was evaluated through the  $\text{NaBH}_4$  hydrolysis at various pH, concentration, and temperature conditions. The reusability of our BCD-AuNPs was examined to prove for its catalytic efficiency and durability.

## 2. Results and Discussion

Beta-cyclodextrin (BCD) is a highly efficient capping agent due to its unique shape [21] which is graphically shown in Figure 1. Consisting mainly of a deep interior hydrophobic chamber capped with a large secondary ring and a smaller primary hydroxyl ring, the molecule exhibits an almost conical shape which aids in restricting particle size [21]. Nanoparticles enter the interior cavity sometime during their formation, then as they continue towards their final morphology, the narrowing walls of the internal cavity can help to restrict the final particle size [21].

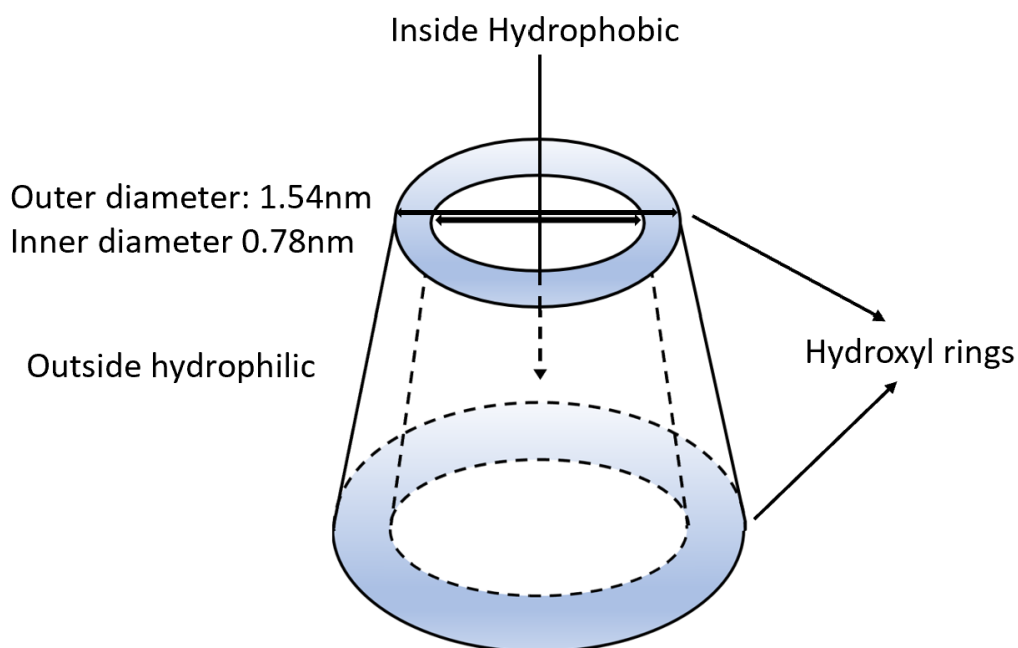


**Figure 1.** An illustration of the beta-cyclodextrin functionality and dimensions.

### 2.1. Characterization

The UV-VIS spectrum (Figure 2) shows the absorbance range between 509 and 520 nm, which indicates the presence of gold nanoparticles [15,22]. The inset shown in Figure 2 is of a cuvette filled with the AuNPs solution.

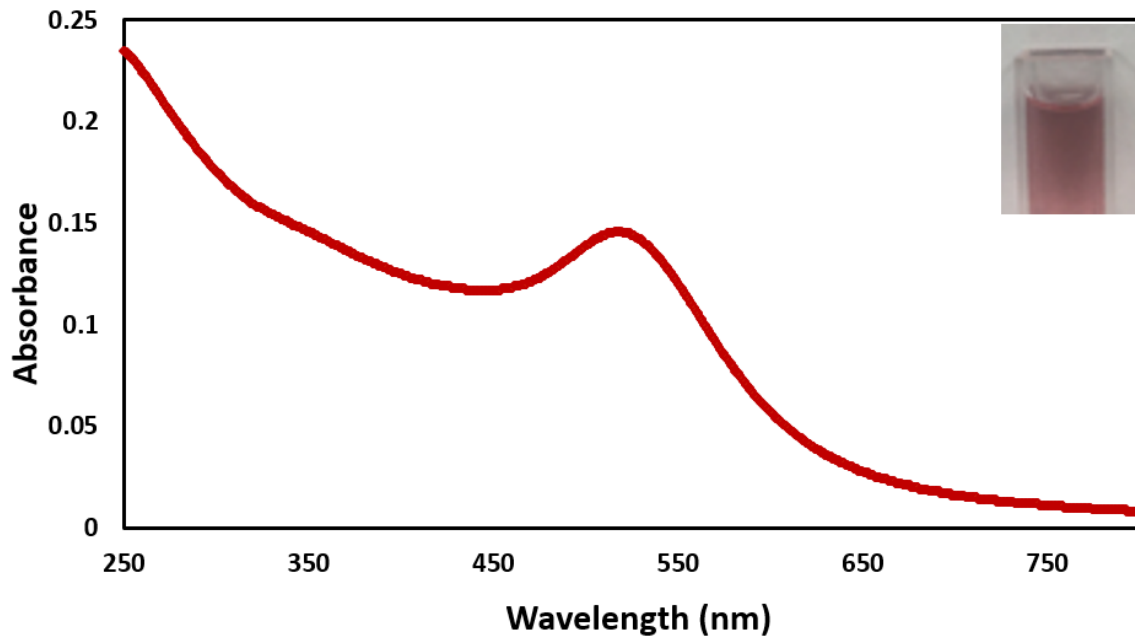


**Figure 2.** UV-Vis spectrum of the BCD–AuNPs. The inset shows the BCD–AuNPs solutions.

Figure 3 displays the crystallinity pattern of AuNPs. Characteristic peaks can be found at  $38.1^\circ$ ,  $44.3^\circ$ ,  $64.6^\circ$ , and  $77.5^\circ$ . These peaks correspond with the (111), (200), (220), and (311) lattice planes of AuNPs. The result is consistent with previously reported studies [23,24]. The other peaks at  $31^\circ$ ,  $56^\circ$ , and  $82^\circ$  were corresponding with the crystal structure of the capping agent, beta-cyclodextrin [25,26].

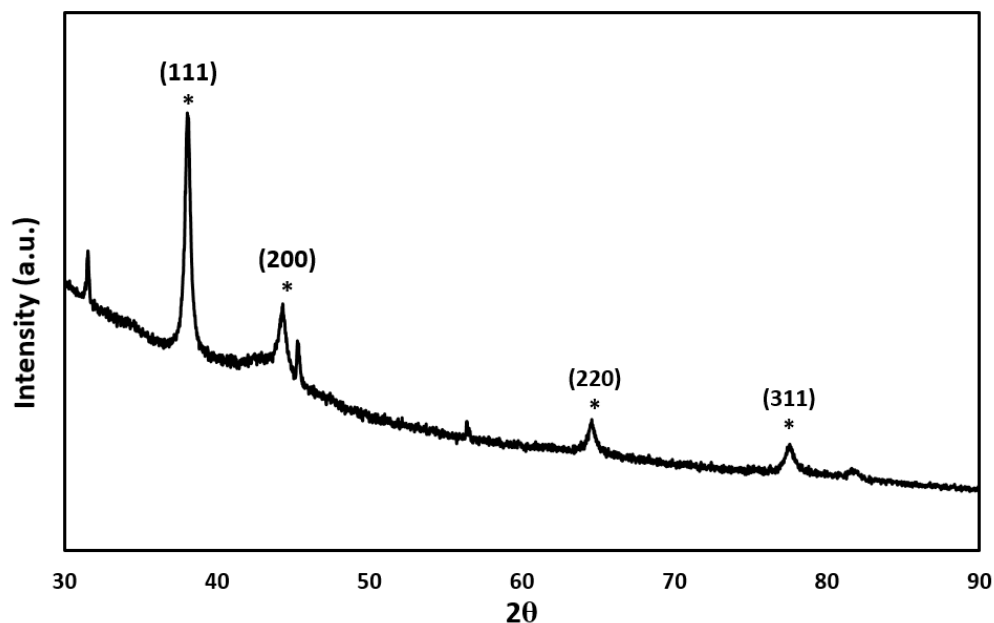


**Figure 3.** P-XRD pattern of gold nanoparticles. The characterized peaks appeared from  $30^\circ$  to  $90^\circ$ . The \* marked the characteristic peaks of gold nanoparticles.

The FTIR spectra pattern of gold nanoparticles solution is shown in Figure 4. The O-H stretch at  $3325\text{ cm}^{-1}$  indicates the presence of hydroxyl group of beta-cyclodextrin [27]. The peaks at  $2900\text{ cm}^{-1}$  and  $1033\text{ cm}^{-1}$  correspond to the CH group and C-O stretching [27,28]. These results confirmed the presence of beta-cyclodextrin within our samples.

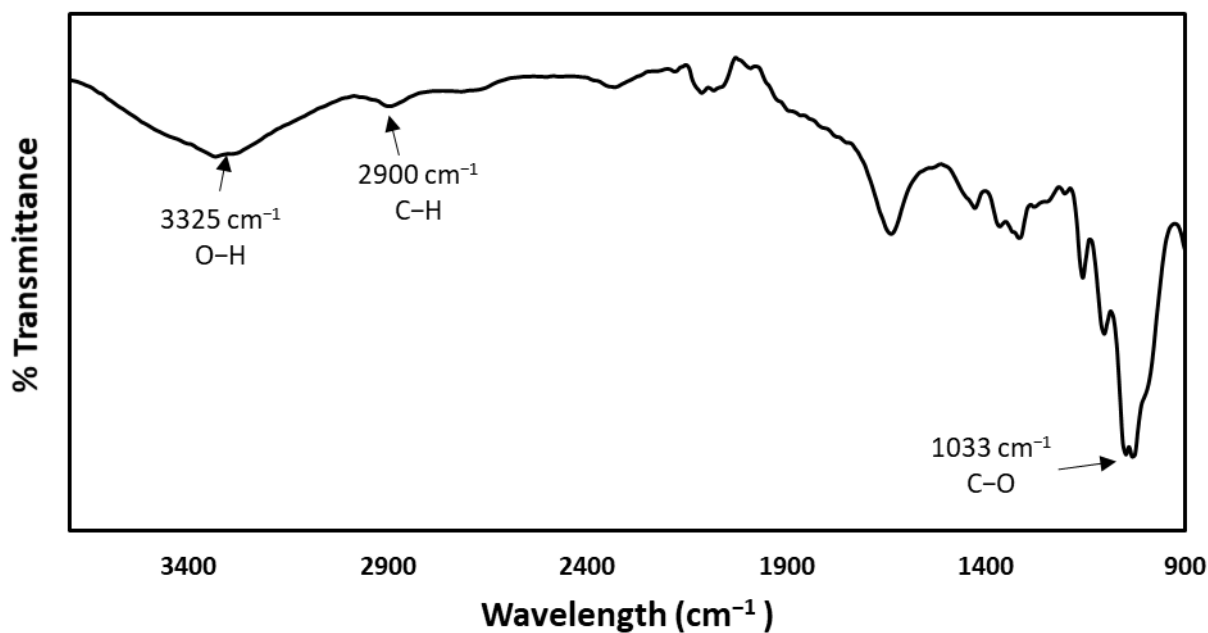


Figure 4. FTIR spectra of BCD–AuNPs.

Figure 5 depicts the TEM micrographs of a network of BCD-AuNPs, with the average size of  $7.7 \pm 3.6$  nm. There was a small agglomeration with a size of approximately 20 nm. The TEM imaging indicated that the beta-cyclodextrin capping matrix which helped to evenly separate and distribute each  $\sim 7.7$  Au nanoparticles in large network of  $\sim 163$  nm by  $\sim 163$  nm as shown in Figure 5 as double headed arrows.

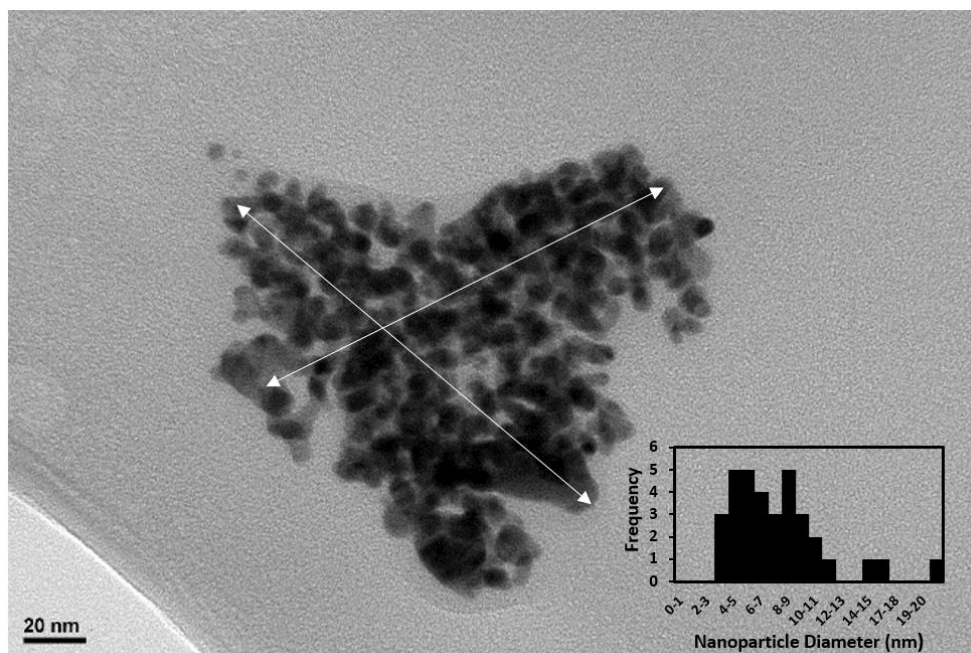
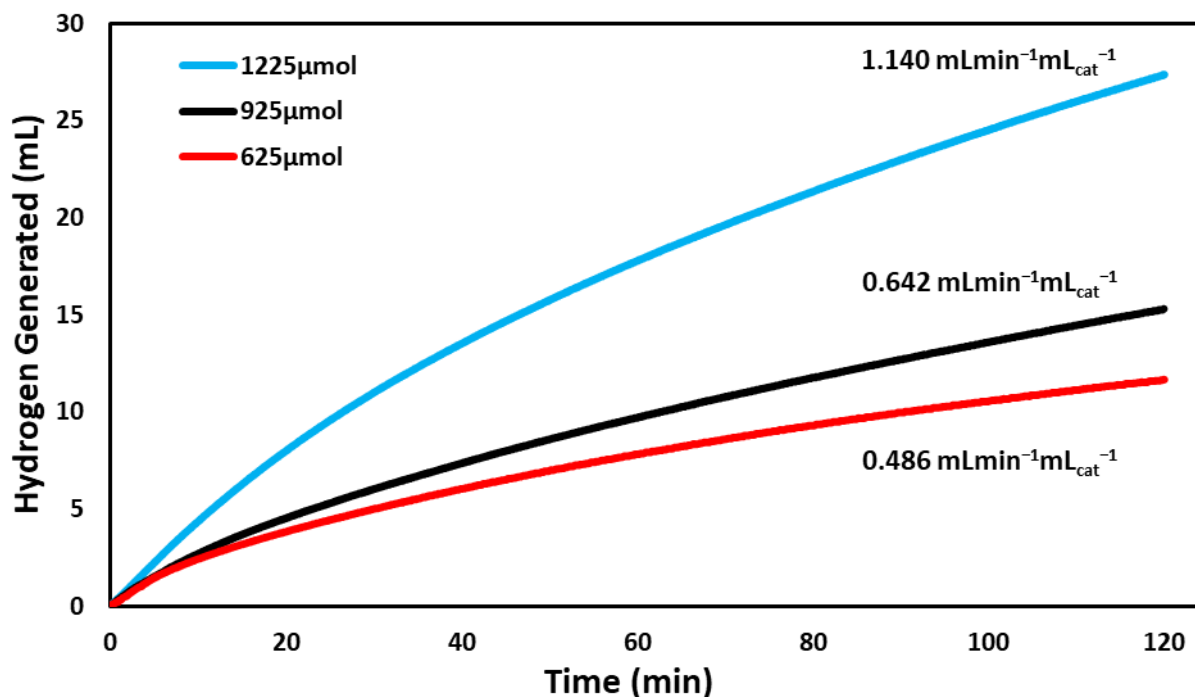


Figure 5. TEM micrograph of the BCD–AuNPs network and an inset showed that the histogram indicated the average diameter of gold nanoparticle is 7.7 nm.

## 2.2. Catalytic Activity with Varied Concentrations of Reactant

Under varied concentrations of reactants, the BCD-AuNPs catalyst evolved hydrogen gas at the fastest rate with 1225  $\mu$ moles of NaBH<sub>4</sub>. The rate of the hydrogen evolution

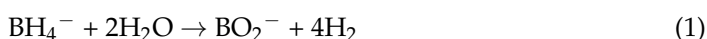
was  $1.140 \text{ mL min}^{-1} \text{ mL}_{\text{cat}}^{-1}$  (Figure 6). The next best concentration for the nanoparticle catalyst was  $925 \mu\text{mol}$ , showing a hydrogen evolution rate of  $0.642 \text{ mL min}^{-1} \text{ mL}_{\text{cat}}^{-1}$ . Lastly,  $625 \mu\text{mol}$  was the concentration with the lowest hydrogen generation rate of  $0.486 \text{ mL min}^{-1} \text{ mL}_{\text{cat}}^{-1}$ . Based on Figure 6, there is a clear trend seen that by increasing the concentration of sodium borohydride, the hydrogen produced also increases. This agrees with Equation (1) and the law of chemical equilibrium where an increase in the reactants causes a shift to increase the products.



**Figure 6.** Comparison of the volume of hydrogen gas generated versus time by the hydrolysis reaction of three different concentrations of sodium borohydride ( $625 \mu\text{mol}$ ,  $925 \mu\text{mol}$ ,  $1225 \mu\text{mol}$ ) as catalyzed by BCD–AuNPs. The reactions were run at  $295 \text{ K}$  and at  $\text{pH } 7$  for roughly  $120 \text{ min}$ .

### 2.3. Catalytic Activity under Varied pH Conditions

When the catalytic activity was tested under varied pH conditions, our BCD-AuNPs catalyst caused the reaction to produce hydrogen gas at the highest rate at a pH of 6, with a rate of  $0.854 \text{ mL min}^{-1} \text{ mL}_{\text{cat}}^{-1}$  (Figure 7). The next best pH condition was pH 7 producing hydrogen at a rate of  $0.642 \text{ mL min}^{-1} \text{ mL}_{\text{cat}}^{-1}$ , and then pH 8 at a rate of  $0.336 \text{ mL min}^{-1} \text{ mL}_{\text{cat}}^{-1}$ . This trend in the rates indicates that the catalyst is pH sensitive, as the reaction is known to proceed faster in lower pH's, due to the production of borate ions during hydrolysis (Equation (1)) [11].



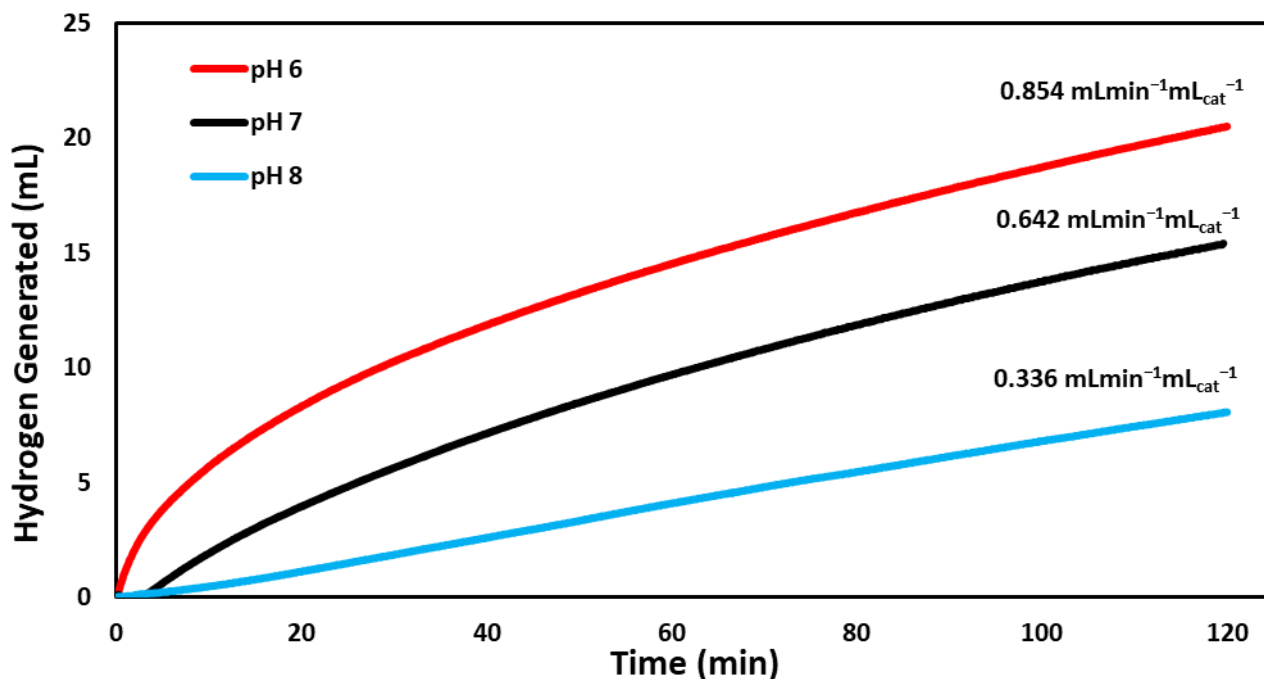


**Figure 7.** Volume of hydrogen gas generated versus time as catalyzed by the BCD–AuNPs under varied pH conditions (pH 6, 7, 8). The reactions were run at 295 K with 925  $\mu$ moles of  $\text{NaBH}_4$  for approximately 120 min.

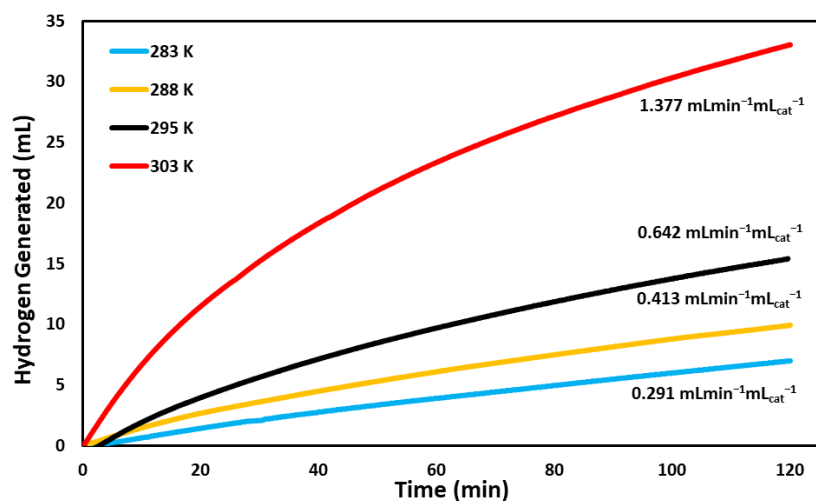
#### 2.4. Catalytic Activity at Varied Temperatures and Activation Energies

Under varied temperatures, BCD-AuNPs produced hydrogen the fastest at 303 K at a rate of  $1.377 \text{ mL min}^{-1} \text{ mL}_{\text{cat}}^{-1}$  (Figure 8). Performance followed 303 K with 295 K, 288 K, and 283 K, producing rates of  $0.642 \text{ mL min}^{-1} \text{ mL}_{\text{cat}}^{-1}$ ,  $0.413 \text{ mL min}^{-1} \text{ mL}_{\text{cat}}^{-1}$ , and  $0.291 \text{ mL min}^{-1} \text{ mL}_{\text{cat}}^{-1}$ , respectively (Figure 8). A clear trend was seen where the rate of hydrogen generation increased with increasing temperatures. According to le Chatelier's principle, this indicates the reaction is endothermic. From the temperature varied trials, activation energy of the gold catalyst was calculated using an Arrhenius plot, and the corresponding equation (Equation (2)). The activation energy of the BCD-AuNPs was determined to be  $54.7 \text{ kJ/mol}$  (Table 1). The nanoparticles network displayed a competitive activation energy when compared to other reported catalysts (Table 1).

$$\ln K = \ln A - E_a/RT \quad (2)$$

where  $\ln K$  is the natural logarithm of rate constant,  $\ln A$  is the natural logarithm of pre-exponential factor,  $E_a$  is the activation energy,  $R$  is the universal gas constant, and  $T$  is the absolute temperature.

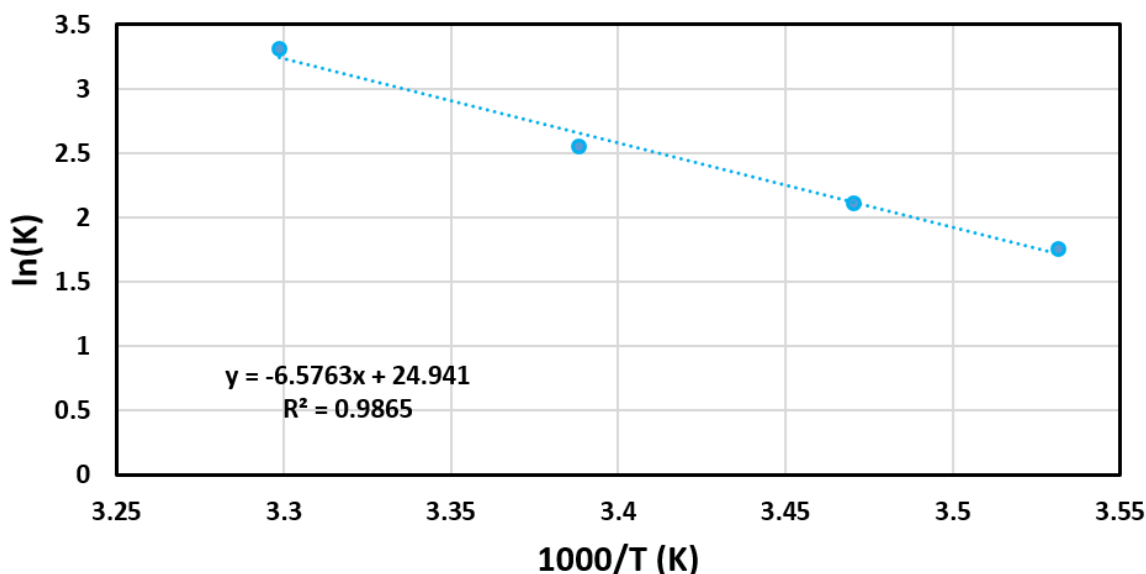
Through the temperature trials (Figure 8), Arrhenius plot (Figure 9), and Equation (2), the activation energy was calculated to be  $54.7 \text{ KJ mol}^{-1}$  and was compared with the activation energy of other catalysts in Table 1. The activation energy of BCD-AuNPs was observed to be lower than unsupported AuNPs [15]. It highly suggested that the dispersion of BCD-AuNPs in the network helped to improve the catalytic ability. Other precious nanoparticles and their composites except PdMWCNT appears to have lower activation energy in comparison to BCD-AuNPs. The BCD-AuNPs had either higher or lower activation energy in comparison to the remaining composites on the table.



**Figure 8.** Volume of hydrogen gas generated by the hydrolysis of  $\text{NaBH}_4$  versus time as catalyzed by the BCD–AuNPs at 283 K, 288 K, 295 K, and 303 K. The reactions were run at pH 7 with 925  $\mu\text{moles}$  of  $\text{NaBH}_4$  for 120 min.

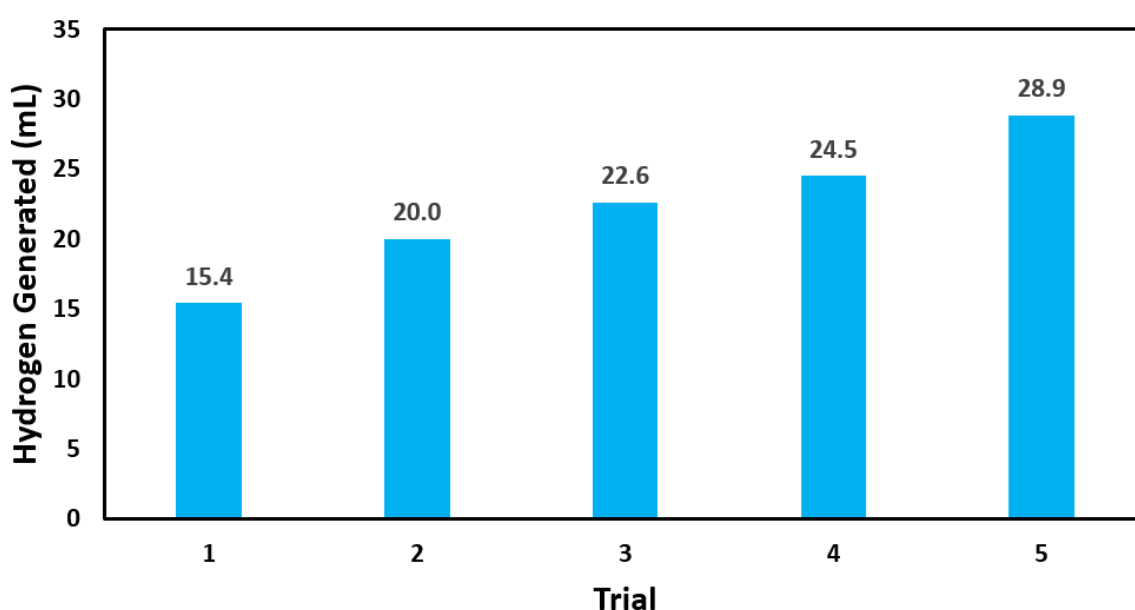
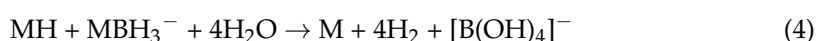
**Table 1.** Reported activation energies for  $\text{NaBH}_4$  hydrolysis by catalyst.

Catalyst	$E_a$ (kJ/mol)	Temperature (K)	Time (min)	Reference
Co@NMGC.	35.2	288–318	2–8	[29]
Co/ $\text{Fe}_3\text{O}_4$ @C	49.2	288–328	30	[30]
Co–Mo–P/CNTs–Ni	47.27	298–313	30	[31]
Co–Cu–B catalyst	52.0	298–318	22	[32]
Co/Ni/MWAC	40.7	30–60	N/A	[33]
CuNW	42.48	298–333	9–250	[34]
Ru/G	61.1	298–318	30	[35]
Cu based catalyst	61.16	293–313	40–130	[36]
$\text{SiO}_2$ @ $\text{H}^+$ PE	32.01	293–323	30–80	[37]
Ag/MWCNTs	44.5	273–303	120	[38]
Au/MWCNTs	21.1	273–303	120	[39]
Unsupported AuNPs	231.7	273–303	120	[15]
AuNPs/AC	21.6	273–308	120	[15]
PdMWCNT	62.6	273–303	120	[40]
PtMWCNT	46.2	283–303	120	[13]
AgNPs	50.3	273–303	120	[41]
PtNPs	39.2	283–303	120	[14]
BCD–AuNPs	54.7	283–303	120	This Work



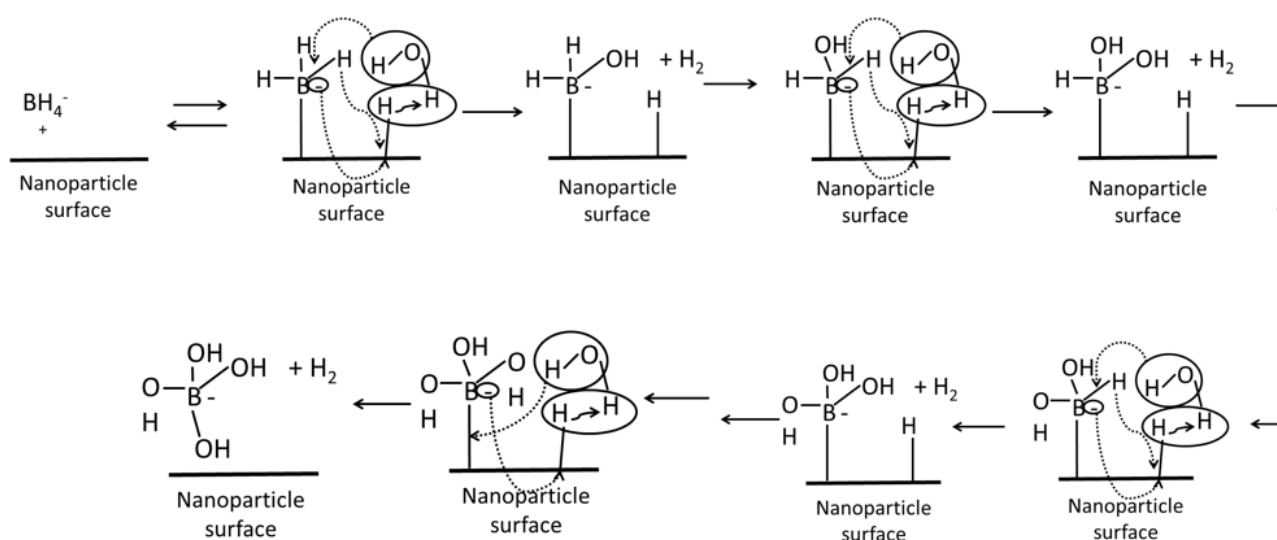
**Figure 9.** Arrhenius Plot used in association with Equation (2) to determine the activation energy of the  $\text{NaBH}_4$  reaction catalyzed by the BCD–AuNPs.

Figure 10 displayed the catalytic reusability of our BCD-AuNPs. The average volume of hydrogen generated across the five trials was 22.3 mL. It was observed that the catalyzed ability of BCD-AuNPs was not diminished with additional uses. The increasing trend of the hydrogen generation could be due to the effect of  $\text{BH}_4^-$  and  $\text{H}^-$  formed strong bonds on the surface of gold nanoparticles, and then over a long period time, these bonds become hydrolyzed and improve the electrostatic stabilization of the AuNPs surface making them more active [42]. These results indicated that BCD-AuNPs are durable and have a potential recyclability for application in hydrogen economy.



**Figure 10.** Catalytic reusability of BCD–AuNPs in the hydrolysis of sodium borohydride. Each trial ran for approximately 2 h under ambient conditions.

The proposed mechanism in Scheme 1 is based on the Michaelis–Menten model for the catalytic hydrolysis of sodium borohydride (Equations (3) and (4)). This mechanism occurs on the nanoparticle surface due to the reaction requiring two metal sites per molecule of borohydride. The borohydride ions anchor on the nanoparticle surface and attracted the hydroxyl group of water molecules. The hydrogen ion is released and combines with free ions. The role of both the occupied and unoccupied catalytic sites is depicted in Scheme 1, and it highly suggested that the dispersion of nanoparticles helps to increase the active surface area. This may offer an explanation to the trends seen in Figure 6, where the gold performed best at the higher concentration due to the increased number of  $\text{BH}_4^-$  attached on the surface of nanoparticles. It should be noted that the mechanism is a multi-electron process between two potential active sites, and thus the catalytic ability of the material to move electrons between adjacent sites is believed to be another important characteristic of a successful catalyst.



**Scheme 1.** Proposed mechanism of the hydrolysis of sodium borohydride as catalyzed by the BCD–AuNPs.

### 3. Materials and Methods

#### 3.1. Synthesis of AuNPs

Chloroauric acid (99.9%, Sigma Aldrich, Saint Louis, MO, USA) was used to create a 1 mM precursor metal solution. The solution was then added to 10 mM aqueous beta-cyclodextrin (99%, Sigma Aldrich, Saint Louis, MO, USA) solution and stirred for ten minutes. A fresh solution of 180 mM  $\text{NaBH}_4$  was then prepared and 0.25 mL of this solution was added to the mixture, and the resulting 134.5  $\mu\text{M}$  metal solution is stirred for 2 h to facilitate nanoparticle formation. Then, the gold nanoparticle solution was centrifuged for 15 min at 14,000 rpm to remove excess reactants, including  $\text{NaBH}_4$ . Therefore, there will be no generation of hydrogen gas in any of the catalytic experiments due to the  $\text{NaBH}_4$  used in the preparation of the catalyst.

#### 3.2. Characterization

Ultraviolet-visible spectroscopy was used to further characterize the samples and verify the presence of nanoparticles. Nanoparticle solutions were characterized in quartz cuvettes using a Shimadzu UV-2600 UV-VIS Spectrophotometer. Deionized Water, 18 M $\Omega$ , (DI) was used as solvent for the reference cell.

The crystal structure of AuNPs was identified by powder X-ray diffraction (P-XRD Rigaku Miniflex II). The presence of capping agent was confirmed through Fourier transform infrared spectroscopy (FTIR, Shimadzu IR-Tracer 100).

The size of gold nanoparticles was determined by transmission electron microscopy (TEM JEM-2100F). As discussed in the synthesis method, DI water is the main solvent for the gold nanoparticles. Then, 1–2 microliters of concentrated gold nanoparticle solution were added onto a TEM sample grid and dried in an oven at a 90 °C overnight.

### 3.3. Catalysis

Catalytic activity of the metal nanoparticles in the evolution of hydrogen from aqueous sodium borohydride was characterized using a gravimetric water displacement system [14,15]. The reaction of 100 mL of deionized water containing 625, 925, and 1125  $\mu\text{mol}$  of  $\text{NaBH}_4$  (J.T. Baker 98%) was catalyzed by using 200  $\mu\text{L}$  of the gold nanoparticle solutions. The catalytic activity was compared in varied pH conditions (pH 6, pH 7, pH 8) and the pH of the solution was adjusted by  $\text{HNO}_3$  and  $\text{NaOH}$ . Activity was also tested at varied temperature conditions (283 K, 288 K, 295 K, and 303 K) which was controlled by a water bath system. The reaction chamber of the system was stirred throughout the reaction to maintain equal distribution of the catalyst and reactant in the solution. The water displaced by the reaction was measured by an Ohaus Pioneer Balance (Pa124) with proprietary mass logging software (SPDC Data logger 2.0, OHAUS 2020). The reaction rate was determined as a product of the overall hydrogen gas produced, the inverse of the duration of the trials (120 min), and the volume of catalyst used. The reusability trials of gold nanoparticles were carried at room temperature and pH 7 for an extended time of 10 h. The authors agree with the journal ethical standards.

## 4. Conclusions

In conclusion a network of BCD-AuNPs was successfully synthesized, and the structure was confirmed by UV-VIS spectroscopy, P-XRD, FTIR, and TEM before it was applied as a catalyst to the hydrogen generation reaction of sodium borohydride. The nanoparticles network performed well as a catalyst for the reaction, performing best at 303 K, producing  $1.377 \text{ mL min}^{-1} \text{ mL}_{\text{cat}}^{-1}$  of hydrogen. It was determined that the activation energy of the reaction, as catalyzed by the produced nanoparticles network, was 54.7 kJ/mol. This activation energy and the reusability results show promise for this material as a stable catalyst for the hydrogen evolution reaction of aqueous sodium borohydride.

**Author Contributions:** Q.Q.: Data curation, Formal analysis, Writing—original draft. E.B.: Data curation, Formal analysis, Writing—original draft. A.E.: Data curation. C.H.: Data curation, Formal analysis, Writing—original draft. J.M.L.: Data curation. T.M.A.-F.: Conceptualization, Validation, Formal analysis, Investigation, Resources, Supervision, Writing—review & editing. All authors have read and agreed to the published version of the manuscript.

**Funding:** This research received no external funding.

**Institutional Review Board Statement:** Not applicable.

**Informed Consent Statement:** Not applicable.

**Data Availability Statement:** The data presented in this study are available on request from the corresponding author.

**Acknowledgments:** Corresponding Author acknowledge Lawrence J. Sacks Professorship in Chemistry.

**Conflicts of Interest:** There is no conflict of interest.

## References

1. Stern, D.I.; Kander, A. The role of energy in the industrial revolution and modern economic growth. *Energy J.* **2010**, *33*, 125–152. [[CrossRef](#)]
2. Morris, A.C.; Nivola, P.S.; Schultze, C.L. Clean energy: Revisiting the challenges of industrial policy. *Energy Econ.* **2012**, *34*, S34–S42. [[CrossRef](#)]
3. Hook, M.; Tang, X. Depletion of fossil fuels and anthropogenic climate change—A review. *Energy Policy* **2013**, *52*, 797–809. [[CrossRef](#)]

4. Bulatov, I.; Klemes, J.J. Clean fuel technologies and clean and reliable energy: A summary. *Clean Technol. Environ. Policy* **2011**, *13*, 543–546. [\[CrossRef\]](#)
5. Mikake, J.; Ogawa, Y.; Tanaka, T.; Ahn, J.; Oka, K.; Oyaizu, K.; Miyatake, K. Rechargeable proton exchange membrane fuel cell containing an intrinsic hydrogen storage polymer. *Commun. Chem.* **2020**, *3*, 138. [\[CrossRef\]](#)
6. Pielke Jr, R.A.; Klein, R.; Maricle, G.; Chase, T.; Keith, D.W. Hydrogen cars and water vapor. *Science* **2003**, *302*, 1329. [\[CrossRef\]](#)
7. Manoharan, Y.; Hossein, S.E.; Butler, B.; Alzahrani, H.; Senior, B.T.F.; Ashuri, T.; Krohn, J. Hydrogen fuel cell vehicles; current status and future prospect. *Appl. Sci.* **2019**, *9*, 2296. [\[CrossRef\]](#)
8. Offera, G.J.; Howey, D.; Contestabile, M.; Clague, R.; Brandon, N.P. Comparative analysis of battery electric, hydrogen fuel cell and hybrid vehicles in a future sustainable road transport system. *Energy Policy* **2010**, *38*, 24–29. [\[CrossRef\]](#)
9. Kalamaras, C.M.; Efstathiou, A.M. Hydrogen production technologies: Current state and future developments. *Conf. Pap. Energy* **2013**, *2013*, 690627. [\[CrossRef\]](#)
10. Hua, T.Q.; Ahluwalia, R.K.; Peng, J.K.; Kromer, M.; Lasher, S.; McKenney, K.; Law, K.; Sinha, J. Technical assessment of compressed hydrogen storage tank systems for automotive applications. *Int. J. Hydrog. Energy* **2011**, *36*, 3037–3049. [\[CrossRef\]](#)
11. Schlesinger, H.; Brown, H.; Finholt, A.; Gilbreath, J.; Hoekstra, H.; Hyde, E. Sodium borohydride, its hydrolysis and its use as a reducing agent and in the generation of hydrogen. *J. Am. Chem. Soc.* **1953**, *75*, 215–219. [\[CrossRef\]](#)
12. Ozkar, S.; Zahmakiran, M. Hydrogen generation from hydrolysis of sodium borohydride using Ru(0) nanoclusters as catalyst. *J. Alloys Compd.* **2005**, *404–406*, 728–731. [\[CrossRef\]](#)
13. Huff, C.; Quach, Q.; Long, J.M.; Abdel-Fattah, T.M. Nanocomposite catalyst derived from ultrafine platinum nanoparticles and carbon nanotubes for hydrogen generation. *ECS J. Solid State Sci. Technol.* **2020**, *9*, 101008. [\[CrossRef\]](#)
14. Huff, C.; Biehler, E.; Quach, Q.; Long, J.M.; Abdel-Fattah, T.M. Synthesis of highly dispersive platinum nanoparticles and their application in a hydrogen generation reaction. *Colloids Surf. A Physicochem. Eng. Asp.* **2021**, *610*, 125734. [\[CrossRef\]](#)
15. Osborne, J.; Horten, M.R.; Abdel-Fattah, T.M. Gold nanoparticles supported over low-cost supports for hydrogen generation from a hydrogen feedstock material. *ECS J. Solid State Sci. Technol.* **2020**, *9*, 071004. [\[CrossRef\]](#)
16. Daniel, M.; Astruc, D. Gold Nanoparticles: Assembly, Supramolecular Chemistry, Quantum-Size-Related Properties, and Applications toward Biology, Catalysis, and Nanotechnology. *Chem. Rev.* **2004**, *104*, 293–346. [\[CrossRef\]](#) [\[PubMed\]](#)
17. Abdel-Fattah, T.M.; Wixtrom, A. Catalytic reduction of 4-Nitrophenol using gold nanoparticles supported on carbon nanotubes. *ECS J. Solid State Sci. Technol.* **2014**, *3*, M18–M20. [\[CrossRef\]](#)
18. Abdel-Fattah, T.M.; Wixtrom, A.; Zhang, K.; Cao, W.; Baumgart, H. Highly uniform self-assembled gold Nanoparticles over high surface area ZnO nanorods as Catalysts. *ECS J. Solid State Sci. Technol.* **2014**, *3*, M61–M64. [\[CrossRef\]](#)
19. Zook, J.M.; Rastogi, V.; MacCuspie, R.I.; Keene, A.M.; Fagan, J. Measuring agglomerate size distribution and dependence of localized surface plasmon resonance absorbance on gold nanoparticle agglomerate size using analytical ultracentrifugation. *ACS Nano* **2011**, *5*, 8070–8079. [\[CrossRef\]](#)
20. Sylvestre, J.; Kabashin, A.V.; Sacher, E.; Meunier, M.; Luong, J.H.T. Stabilization and size control of gold nanoparticles during laser ablation in aqueous cyclodextrins. *J. Am. Chem. Soc.* **2004**, *126*, 7176–7177. [\[CrossRef\]](#)
21. Geze, A.; Aous, S.; Baussanne, I.; Putaux, J.; Defaye, J.; Wouessidjewe, D. Influence of chemical structure of amphiphilic  $\beta$ -cyclodextrins on their ability to form stable nanoparticles. *Int. J. Pharm.* **2002**, *242*, 301–305. [\[CrossRef\]](#)
22. Haiss, W.; Thanh, N.T.K.; Aveyard, J.; Fernig, D.G. Determination of size and concentration of gold nanoparticles from UV–Vis spectra. *Anal. Chem.* **2007**, *79*, 4215–4221. [\[CrossRef\]](#)
23. Khalil, M.M.H.; Ismail, E.H.; El-Magdoub, F. Biosynthesis of Au nanoparticles using olive leaf extract: 1st nano updates. *Arab. J. Chem.* **2012**, *5*, 431–437. [\[CrossRef\]](#)
24. Krishnamurthy, S.; Esterle, A.; Sharma, N.C.; Sahi, S.V. Yucca-derived synthesis of gold nanomaterial and their catalytic potential. *Nanoscale Res. Lett.* **2014**, *9*, 627. [\[CrossRef\]](#) [\[PubMed\]](#)
25. A Bocanegra-Diaz, N.D.S.; Mohallem, R.D.S. Preparation of a ferrofluid using cyclodextrin and magnetite. *J. Braz. Chem. Soc.* **2003**, *14*, 1678–4790. [\[CrossRef\]](#)
26. Sarfraz, R.M.; Ahmad, M.; Mahmood, A.; Akram, M.R.; Abrar, A. Development of  $\beta$ -cyclodextrin-based hydrogel microparticles for solubility enhancement of rosuvastatin: An in vitro and in vivo evaluation. *Drug Des. Dev. Ther.* **2017**, *2017*, 3083–3096. [\[CrossRef\]](#)
27. Sambasevam, K.P.; Mohamad, S.; Sarih, N.M.; Ismail, N.A. Synthesis and characterization of the inclusion complex of  $\beta$ -cyclodextrin and azomethine. *Int. J. Mol. Sci.* **2013**, *14*, 3671–3682. [\[CrossRef\]](#)
28. Rachmawati, H.; Edityaningrum, C.A.; Mauludin, R. Molecular inclusion complex of curcumin– $\beta$ -Cyclodextrin nanoparticle to enhance curcumin skin permeability from hydrophilic matrix gel. *AAPS PharmSciTech* **2013**, *14*, 1303–1312. [\[CrossRef\]](#)
29. Li, J.; Hong, X.; Wang, Y.; Luo, Y.; Huang, P.; Li, B.; Zhang, K.; Zou, Y.; Sun, L.; Xu, F.; et al. Encapsulated cobalt nanoparticles as a recoverable catalyst for the hydrolysis of sodium borohydride. *Energy Storage Mater.* **2020**, *27*, 187–197. [\[CrossRef\]](#)
30. Chen, B.; Chen, S.; Bandal, H.A.; Appiah-Ntiamoah, R.; Jadhav, A.R.; Kim, H. Cobalt nanoparticles supported on magnetic core-shell structured carbon as a highly efficient catalyst for hydrogen generation from NaBH<sub>4</sub> hydrolysis. *Int. J. Hydrog. Energy* **2018**, *43*, 9296–9306. [\[CrossRef\]](#)
31. Wang, F.; Zhang, Y.; Luo, Y.; Wang, Y.; Zhu, H. Preparation of dandelion-like Co–Mo–P/CNTs–Ni foam catalyst and its performance in hydrogen production by alcoholysis of sodium borohydride. *Int. J. Hydrog. Energy* **2020**, *45*, 30443–30454. [\[CrossRef\]](#)

32. Wang, Y.; Zou, K.; Zhang, D.; Cao, Z.; Zhang, K.; Xie, Y.; Zhou, G.; Li, G.; Bai, S. Cobalt–copper–boron nanoparticles as catalysts for the efficient hydrolysis of alkaline sodium borohydride solution. *Int. J. Hydrog. Energy* **2020**, *45*, 9845–9853. [[CrossRef](#)]
33. Soltani, M.; Zabihi, M. Hydrogen generation by catalytic hydrolysis of sodium borohydride using the nano-bimetallic catalysts supported on the core-shell magnetic nanocomposite of activated carbon. *Int. J. Hydrog. Energy* **2020**, *45*, 12331–12346. [[CrossRef](#)]
34. Hashimi, A.S.; Nohan, M.A.N.M.; Chin, S.X.; Khiew, P.S.; Zakaria, S.; Chia, C.H. Copper nanowires as highly efficient and recyclable catalyst for rapid hydrogen generation from hydrolysis of sodium borohydride. *Nanomaterials* **2020**, *10*, 1153. [[CrossRef](#)] [[PubMed](#)]
35. Liang, Y.; Dai, H.; Ma, L.; Wang, P.; Cheng, H. Hydrogen generation from sodium borohydride solution using a ruthenium supported on graphite catalyst. *Int. J. Hydrog. Energy* **2020**, *35*, 3023–3028. [[CrossRef](#)]
36. Balbay, A.; Saka, C. Effect of phosphoric acid addition on the hydrogen production from hydrolysis of NaBH<sub>4</sub> with Cu based catalyst. *Energy Source Part A* **2018**, *40*, 794–804. [[CrossRef](#)]
37. Yang, L.; Huang, X.; Zhang, J.; Dong, H. Protonated poly(ethylene imine)-coated silica nanoparticles for promoting hydrogen generation from the hydrolysis of sodium borohydride. *ChemPlusChem* **2020**, *85*, 399–404. [[CrossRef](#)]
38. Huff, C.; Long, J.M.; Aboulatta, A.; Heyman, A.; Abdel-Fattah, T.M. Silver nanoparticle/multi-walled carbon nanotube composite as catalyst for hydrogen production. *ECS J. Solid State Sci. Technol.* **2017**, *6*, M115. [[CrossRef](#)]
39. Huff, C.; Dushatinski, T.; Abdel-Fattah, T.M. Gold nanoparticle/multi-walled carbon nanotube composite as novel catalyst for hydrogen evolution reactions. *Int. J. Hydrog. Energy* **2017**, *42*, 18985–18990. [[CrossRef](#)]
40. Huff, C.; Long, J.M.; Heyman, A.; Abdel-Fattah, T.M. Palladium nanoparticle multiwalled carbon nanotube composite as catalyst for hydrogen production by the hydrolysis of sodium borohydride. *ACS Appl. Energy Mater.* **2018**, *1*, 4635–4640. [[CrossRef](#)]
41. Huff, C.; Long, J.M.; Abdel-Fattah, T.M. Beta-cyclodextrin-assisted synthesis of silver nanoparticle network and its application in a hydrogen generation reaction. *Catalysts* **2020**, *10*, 1014. [[CrossRef](#)]
42. Deraedt, C.; Salmon, L.; Gatard, S.; Ciganda, R.; Hernandez, E.; Ruiz, J.; Astruc, D. Sodium borohydride stabilizes very active gold nanoparticle catalysts. *Chem. Commun.* **2014**, *50*, 14194–14196. [[CrossRef](#)] [[PubMed](#)]